Available online at www.sciencedirect.com
SCIENCE DIRECT
Polymer 46 (2005) 8689–8702
polymer
www.elsevier.com/locate/polymer

Molecular simulation of crystal growth in long alkanes

N. Waheed, M.J. Ko, G.C. Rutledge*

Department of Chemical Engineering, Massachusetts Institute of Technology, Room 66-368, 77 Massachusetts Avenue, Cambridge, MA 02139, USA

Received 9 September 2004; received in revised form 31 January 2005; accepted 2 February 2005
Available online 1 July 2005

Abstract

We report crystal growth rate data from the melt for C50 and C100 obtained from non-equilibrium molecular dynamics simulations. This extends our previous results for *n*-eicosane (C20) [Waheed et al. J Chem Phys 2002;116:2301]. We also construct a crystal growth model that accounts for the thermodynamic driving force and relaxation time, using WLF theory and a small number of chemically specific quantities that can be estimated from molecular dynamics simulations. Our model can predict growth rates as a function of temperature and molecular weight, up to the entanglement molecular weight. Qualitatively, we see frequent adsorption and desorption of chain segments on the surface in both C50 and C100 systems. We find evidence for a surface nucleus involving 4–5 chain segments that are approximately 20 beads long, shorter than the ultimate thickness of the chain stem in the crystal, and involving segments from multiple chains. Treatment of relaxation dynamics using the Rouse model and the reptation model does not yield a statistically significant difference within the limits of our data, but the Rouse-based fit yields thermodynamic parameters that are in closer accord with those found from fits to experiments.

Keywords: Crystallization; Molecular dynamics; Alkane

1. Introduction

Molecular simulation has become a very powerful tool for understanding the process of alkane crystallization. Simulation techniques such as lattice dynamics, Monte Carlo, and molecular dynamics provide detailed information that experiments have not yet been able to capture, due to temporal and spatial resolution limitations of the experimental techniques and the complications that arise in the analyses of the complex morphologies of crystallizing polymer systems. Through carefully constructed simulations, one can independently observe nucleation [1–4] and growth [5–8] during melt crystallization, the latter often described as either layer or normal growth.

In an earlier report, we presented results from non-equilibrium molecular dynamics simulations for crystal growth rates of n-eicosane ($C_{20}H_{42}$, denoted here as C20), as a first attempt to understand crystallization in polyethylene, the prototypical polymer [8]. By simulating growth on a pre-existing crystal surface under isothermal conditions (appropriate for cases, where heat transfer away from the crystallization front occurs much faster than the progression of the front itself), we avoided the long waiting times associated with primary homogeneous nucleation and directly observed the rate of growth of the *n*-alkane crystal.

Phenomenologically, one observes a maximum growth rate at a temperature intermediate between the glass transition temperature T_g and the melt temperature T_m. This arises as a competition between a thermodynamic driving force towards crystal growth, associated with locking chains into crystallographic registry and which is rate limiting at high temperatures, and the ability of chains to diffuse to the new layer and rearrange themselves conformationally to satisfy the restrictions of crystal symmetry, which is rate limiting at low temperatures.

In experiment and modeling of the kinetics of alkane crystallization, focus has been concentrated on growth rates very near the melting temperature, where the growth of these systems is optically observable. In this temperature range near T_m, diffusion is not a limiting factor, which has led to theory that accurately models the thermodynamic driving force and its effect on kinetics [9,10]. This also allows for studying the effects of chain length by considering its effects on the melting temperature.

However, using molecular simulation, we are able to

* Corresponding author. Tel.: +1 617 253 0171; fax: +1 617 258 8992.
E-mail address: rutledge@mit.edu (G.C. Rutledge).

0032-3861/$ - see front matter © 2005 Elsevier Ltd. All rights reserved.
doi:10.1016/j.polymer.2005.02.130

observe growth for a range of temperatures around the temperature at which the maximum growth rate occurs. Under these conditions, previous models for alkane crystallization kinetics do not suffice since they generally do not account for the reduced mobility at low temperature [11]. Models for the kinetics of polymer crystallization are more capable of capturing this temperature dependence, because it is a combination of thermodynamics and the constraints of diffusion and chain connectivity that lead to the unique chain-folded lamellar structure of melt-crystallized polymers. However, growth kinetics are not particularly sensitive to molecular weight for long, entangled chains, and, therefore, polymer growth rate models typically do not often have explicit molecular weight dependence.

For polymer crystallization, lamellar growth rates have been shown to exhibit a temperature dependence which matches that of the radial spherulitic growth rate, which in turn has led to the correspondence between spherulitic crystal growth and that of individual lamellae [12]. Growth rates are of interest to the processing community, who require accurate crystallization kinetic data over the entire temperature range, in order to predict solidification under process conditions and final fiber properties.

Several previous models have been suggested to account for the temperature dependence of polymer linear growth rates, based on different approaches. Based purely on empirical evidence, Ziabicki modeled the dependence by using a simple Gaussian function; this has become the standard model in polymer fiber processing [13]. There are several other approaches that have invoked a combination of theory and empirical fitting. Gandica and Magill noted that a corresponding states equation existed for crystallization kinetics, whereby almost all data could be reduced to a dimensionless 'master curve,' described by the maximum growth rate, the melt temperature, and the glass transition temperature [14]. Recent work by Umemoto and Okui has extended this approach by using theory to yield a general analytical form for the master curve and solving for the maximum growth rate as a function of molecular weight [15]. Van Krevelen followed a similar approach, using both theory and empirical data, but was unable to find an equation that would model satisfactorily the diffusion term over the entire range of supercoolings [16].

Purely theoretical approaches have been based on classical nucleation theory and vary according to the concept of nucleation employed. While our simulations are not yet equipped to parameterize such detailed equations, they can provide insight into the validity of the assumptions used in the models. The most sophisticated model of secondary nucleation is that due to Hoffman and co-workers, in which the crystallization process is limited by the attachment of the first fully extended stem or, in later work, localization of an adsorbed but unattached segment to a smooth surface of the crystal [9,17]. Lauritzen and Hoffman have extended this theory to large undercoolings [18]. Three different regimes of growth have been predicted and modeled for polyethylene [19]. Shorter chain lengths favor what Hoffman termed regimes I and II growth, where deposition occurs within a single layer. For the undercoolings relevant to processing, however, the phenomena observed are comparable to what Hoffman termed regime III growth, or rough growth, where new chains nucleate on steps, terraces, or kinks on the crystal surface. Mandelkern also developed a model based on the idea that the formation of a critical monomolecular nucleus is the limiting step in the crystallization process [10]. Binsbergen provided early criticism of both approaches [20]. In particular, he argued that Hoffman's assumption that the critical nucleus is a fully extended chain ignores the fact that there are lower energy paths to creating a new layer. Also, he questioned whether Mandelkern's assumption of an easily defined surface nucleus makes sense, in light of the random attachment and removal of segments that he believed would occur. These criticisms were consistent with theories of growth suggested by Point [21] and by Sadler and Gilmer [22], in which the crystallizing surface might sample several conformations before finding one that is stable and contributes to growth. Keller et al. suggested that the presence of a stable, highly mobile hexagonal phase for polyethylene at high pressure might be indicative of an intermediate mobile phase at the growth front that is capable of lamellar thickening, in addition to lateral growth [23]. More recently, Strobl has introduced a model for crystal growth, where a layer of 'granular crystals,' which develop from a 'mesomorphic' layer of highly ordered melt, precedes the formation of the final lamella [24].

None of these models are fully capable of describing alkane crystallization rates over a wide range of temperatures and molecular weights solely using parameters that depend only on chemical architecture. Nevertheless a model that retains its connection to molecular structure would certainly be of benefit for purposes of product design; such connection is possible using molecular simulations. In this work, we attempt to retain this connection by extracting meaningful rate parameters based on our molecular dynamics results, with the goal being to provide rate data that could be used in a continuum level model of crystallization during fiber or film processing. To our knowledge, this is the first such attempt to parameterize a crystallization rate equation from simulations at the molecular level. In addition, a molecular level approach can possibly corroborate the assumptions of the many conceptions of polymer surface nucleation, as well as their predictions.

We use the same non-equilibrium molecular dynamics (NEMD) technique as was used previously for C20 [8]. In this work, we consider systems of the longer alkanes $C_{50}H_{102}$ and $C_{100}H_{202}$, denoted C50 and C100, for the purpose of studying the molecular weight dependence of the crystal growth rate and to investigate additional characteristics of the growth process, such as chain folding, that are

observed in polyethylene crystallization, but that were not observed in our n-eicosane simulations.

It is worth noting that these simulations are considerably more time-consuming than those for C20, not only due to the larger simulation cells required in order to avoid artifacts of the finite simulation cell size, but also due to the longer simulation times required in order to capture the slower crystallization kinetics. Despite these limitations, molecular dynamics, through its resolution on the atomic length scale, provides information that cannot be obtained through any other source. Therefore, it is our goal to use the atomic scale information provided by molecular dynamics to parameterize a phenomenological model of polymer crystal growth that accounts for both temperature and molecular weight dependence and does not rely on experimental sources to parameterize chemical constants.

2. Method

2.1. Crystallization rate model

To recap our earlier report, our results for C20 were readily described by an empirical equation due to Ziabicki:

$$G = G_{\max}\exp\left[-4\log 2\frac{(T-T_{\max})^2}{D^2}\right] \quad (1)$$

where $G_{\max}$ is the maximum growth rate, $T_{\max}$ is the temperature at which it occurs, and D is the half-width of the Gaussian curve [13]. However, despite its success in capturing the temperature dependence of the crystallization rate, it does not account for the effects of molecular weight or provide any connection to the underlying phenomena. To accomplish this, we develop the analytical form of the crystallization model from scratch, following the arguments described above in connection with combined theoretical/experimental models.

To start, we take the usual step [9,16], originally suggested by Turnbull and Fisher [25], of decomposing the energy barrier into a thermodynamic part for the formation of a critical nucleus and a diffusive part for activated diffusion to the phase boundary. This allows for the parameterization of the growth rate G in terms of energy barriers to nucleation and diffusive hopping:

$$G = G_0\exp\left[-\frac{E_D}{RT}\right]\exp\left[-\frac{\Delta G_2^*}{RT}\right] \quad (2)$$

where G_0 is a pre-factor, E_D is the barrier to diffusive hopping, and ΔG_2^* is the free energy required to form a critical two-dimensional surface nucleus. Much of the prior work in this field has focused on the second, thermodynamic term, which was formulated for a spherical drop by Gibbs [26], and generalized by Turnbull and Fischer. The temperature dependence of this term is readily observed close to the melting point, where the process of crystallization is nucleation-limited. For polyethylene close to T_m [27], Mandelkern et al. observed the following proportionality,

$$G \propto \exp\left[\frac{-K_g}{T\Delta T}\right] \quad (3)$$

where K_g is the surface nucleation constant reflecting the ratio of surface energy to bulk energy of a critical volume, and ΔT is $(T_m - T)$, the undercooling below the equilibrium melting temperature. This constant K_g is a consequence of general nucleation theory and is relatively independent of molecular weight, since the surface energies and free energy difference between the subcooled amorphous and crystal phase are functions of the chemical properties of the monomer unit only. This result was derived theoretically for a general description of surface nucleation in polymers by Binsbergen [20], and was applied to specific models of a surface nucleus by Hoffman and Weeks [9] and by Mandelkern [10].

The diffusive term, on the other hand, has not been parameterized for alkanes; for polymers, it has been difficult to find a relation that applies over a large temperature range. Using Eq. (2), and the empirical data of Mandelkern et al. for E_D [27], van Krevelen proposed a crystallization rate equation of the form:

$$G = G_0\exp\left[-C_D\frac{T_m^2}{T(T_m - T_g)}\right]\exp\left[-\frac{C}{T}\left(\frac{T_m}{T_m - T}\right)\right] \quad (4)$$

where G_0 is 10^{12} nm/s, C_D is a dimensionless constant with a value of approximately 5 for most polymers, and C is a characteristic constant for every polymer, containing the ratio of the surface energy of a nucleus to the lattice energy gained by crystallization [16]. In this equation, the competing forces of secondary nucleation and thermal diffusion are described in terms of T_m, the thermodynamic melting point of a perfect crystal, and T_g, the glass transition temperature, where diffusive motion is arrested, respectively. One feature of this model is that it allows for asymmetric curves for growth rate versus temperature, something that Ziabicki's empirical form does not capture. However, this equation has not been applied to both the diffusion-limited and thermodynamically-limited regions, because of the inability to parameterize the diffusive term over the entire temperature range. In addition, while there has been some work to characterize the molecular weight dependence of G_0 [28], we wish to provide here a more fundamental basis. Hoffman observed that E_D should be described by a Williams–Landel–Ferry (WLF) function for $T_g < T < T_g + 100$ K [9], but invoked an Arrhenius relationship for temperatures close to the melting point.

The original concept for the diffusive energy barrier in Eq. (2) was the free energy of activation for short-range diffusion of atoms moving a fraction of the atomic distance to join the lattice [25]. In the limit that the free energy of crystallization is large and negative, the thermodynamic

term becomes negligible, and the rate of crystallization is diffusion-limited. In classical reaction rate theory, a diffusion limited reaction is parameterized in terms of the self-diffusion constant D.

However, in alkane and polymer crystallization is it not necessarily the translation of species towards the surface that yields the predominant energy barrier, but rather the conformational rearrangement (e.g. extension) of the chains at the surface. To capture this, we parameterize the equation as a function of the relaxation time of the segment of the chain required for surface nucleation. This is the simplest quantity that captures diffusive mobility for which the temperature and molecular weight dependence is understood. There are two factors that influence mobility: the chemical properties of the monomer unit, and the number of monomer units in the chain. Previous models have not explicitly accounted for this fact, since for high molecular weight polymers, the molecular weight dependence has proven difficult to quantify. The molecular weight dependence of the overall growth rate of entangled polymer chains remains a matter of debate, with power law exponents ranging from -0.5 to -1.8, often depending on the temperature range [29]. For low molecular weights of the order of $M_w = 10^4$ g/mol, the scatter in the experimental data has made it difficult to determine a relation [30]. However, for alkanes, by parameterizing in terms of the relaxation time, we can account for both temperature and molecular weight dependences. The mobility term is described by the term G_0, which is the diffusion-limited rate for a reference chain, τ_0, the relaxation time for the reference chain at some reference temperature, and τ, the relaxation time at the temperature and molecular weight of interest. The mobility is related to the reference chain by a ratio of relaxation times. The temperature and molecular weight dependence of the thermodynamic term is well described by the second exponential factor in Eq. (4). Combining the two contributions results in a growth rate given by

$$G(T,N) = G_0\left(\frac{\tau_0}{\tau(T,N)}\right)^n \exp\left[-\frac{C}{T}\left(\frac{T_m(N)}{T_m(N)-T}\right)\right] \quad (5)$$

where the exponent n is included to account for uncertainty regarding the dependence of crystallization rate on relaxation time.

The relevant relation for the relaxation time near a crystallizing surface is not clear from the literature. In particular, the debate centers on the behavior of the amorphous material near the crystal surface. It is generally agreed that diffusion near a surface is more complex than bulk diffusion [31]; however, the way in which the surface affects dynamics is still a matter of debate. Some researchers argue that the surface diffusion rates for short chains near a surface can be described by Rouse dynamics, where the relaxation time should have a power law dependence of 2 in molecular weight [32]. However, there is some indication that relaxation times of polymer chains near surfaces exhibit a power law dependence of 3 in molecular weight, indicating that chains with a 2D conformation behave more like reptating chains than Rouse chains [33].

Furthermore, a crystallizing surface is not the same as a static surface, since it is constantly converting amorphous material to crystal, and thus moving the surface forward in accord with the chain conformation rather than requiring the amorphous chains to conform to the (usually flat) shape of the surface. By this argument, the amorphous material near the surface still diffuses as in the bulk, where for chains below the entanglement length (approximately 150 beads), Rouse dynamics are expected. Rather than committing to either assumption, we analyze our NEMD data here according to both the Rouse and reptation models for relaxation time.

According to Rouse theory, the longest relaxation time of a polymer chain is given by:

$$\tau_R = \frac{N^2 b^2 \zeta_0}{3\pi^2 kT} \quad (6)$$

where N is the degree of polymerization, b is the monomer diameter, T is temperature and ζ_0 is the monomeric friction coefficient. The Rouse formulation applies to short chains in an unentangled melt. Reptation dynamics, which are observed in entangled systems, have a relaxation time given by the following,

$$\tau_D = \frac{N^3 b^4 \zeta_0}{\pi^2 kTa^2} \quad (7)$$

where a is a primitive segment length, defined as the distance between entanglements. In both Rouse and reptation dynamics, the relaxation time can be captured by the following general relation,

$$\tau(T,N) = \frac{C_\tau N^m \zeta_0}{T} \quad (8)$$

where C_τ is the constant containing the geometric and physical factors, and m is the molecular weight dependence, which is 2 for Rouse dynamics and 3 for reptation dynamics.

In a melt, ζ_0 represents the force per unit velocity required to move a monomeric unit through a sea of similar polymer chains, and thus is itself dependent on both temperature and molecular weight of the polymer [34]. The monomeric frictional force is closely related to the free volume associated with a monomer unit in the melt, and, therefore, exhibits a temperature dependence described by the Williams–Landel–Ferry (WLF) equation:

$$\ln\left(\frac{\zeta_0}{\zeta_{0g}}\right) = -\frac{2.303 c_1 (T - T_g)}{c_2 + (T - T_g)} \quad (9)$$

where the WLF constants c_1 and c_2 are 17.44 and 51.66 K, respectively [35]. The monomeric friction coefficient at the glass transition temperature is ζ_{0g}, which has negligible dependence on molecular weight. The free volume at the

glass transition temperature is considered a universal parameter, because it represents an iso-free-volume state; similarly ζ_{0g} should be the same for any polymer at its glass transition point [34].

By inserting Eq. (9) into Eq. (8), we find that the ratio of relaxation times takes the following form,

$$\frac{\tau_0}{\tau(T,N)} = \left(\frac{N_0}{N}\right)^m \exp\left[\frac{2.303c_1(T-T_g)}{c_2+(T-T_g)}\right] \tag{10}$$

where τ_0 is the relaxation time of a reference chain of a certain molecular weight at the glass transition temperature. The ratio of temperatures from Eq. (8) has been dropped, as is done in WLF theory, because it is a lower-order dependence and contributes negligibly to the temperature dependence of relaxation time. Inserting Eq. (10) into Eq. (5), we obtain the following final equation for the linear growth rate:

$$G(T,N) = G_0\left(\frac{N_0}{N}\right)^{mn} \exp\frac{2.303nc_1(T-T_g(N))}{c_2+(T-T_g(N))} \times \exp\left[-\frac{C}{T}\left(\frac{T_m(N)}{T_m(N)-T}\right)\right] \tag{11}$$

This results in a diffusive term that has a WLF dependence, now adjusted by n. By tracing the WLF dependence to the relaxation time, Eq. (11) obtains its molecular weight dependence. In addition to the explicit temperature dependence given by Eq. (11), the molecular weight also enters the equation implicitly through the glass transition temperature and through the melting temperature. Although the Fox–Flory equation is usually used to relate the glass transition and molecular weight, it does not hold for low molecular weights. Therefore, we use an alternative equation presented by Fox and Loshaek [36], which does not present singularities at low molecular weights:

$$\frac{1}{T_g(N)} = \frac{1}{T_g^\infty} + \frac{C_g}{\left(T_g^\infty\right)^2}\frac{1}{N} \tag{12}$$

where T_g^∞ is the asymptotic value of T_g at infinite molecular weight, and C_g is a constant. Data on molecular weight dependence of the melting temperature have been tabulated [37] and are found to fit to the same form:

$$\frac{1}{T_m(N)} = \frac{1}{T_m^\infty} + \frac{C_m}{\left(T_m^\infty\right)^2}\frac{1}{N} \tag{13}$$

where T_m^∞ is the asymptotic value of T_m at infinite molecular weight and C_m is a constant. The constants C_g and C_m are consequences of the chemical properties of the monomer. Molecular simulation can be used to determine these constants through a series of simulations. Methodology for these simulations has been described elsewhere [3,8]. However, due to the large number of simulations that would be required to model the dependency, in this work we have treated them as fitting parameters in the solving of the rate equation, which results in three fitting parameters for Eq. (11), G_0, C, and n, and the four parameters that characterize the molecular weight dependence of the melting and glass transition temperatures, from Eqs. (12) and (13).

2.2. Computational method

A united atom interaction potential is used, in which polymer chains are represented by CH_2 and CH_3 beads that interact through bonded and non-bonded interactions. Previously, we have shown the importance of using realistic potentials in modeling this process [2]. Accurate values for the barriers between torsional states are essential in capturing the balance between the orienting process and the crystal packing process. It is the proper balance of these forces that allows one to determine correctly which of several credible mechanisms is the pathway to loop formation. Therefore, our research focuses on modeling the process using potentials that are well-parameterized for polyethylene melt dynamics. We use the interaction parameters for angles, torsions, and excluded volume interactions calibrated by Paul et al. for united atom polyethylene, where CH_2 and CH_3 beads behave identically [38]. The total potential E_{TOTAL} consists of several terms:

$$E_{TOTAL} = E_{BOND} + E_{ANGLE} + E_{TORSION} + E_{NONBOND} \tag{14}$$

The harmonic bond length potential E_{BOND} for bonded atoms is given by

$$E_{BOND} = k_b(r - r_{eq})^2 \tag{15}$$

where $k_b = 350$ kcal/mol Å^2 and $r_{eq} = 1.53$ Å. The harmonic bond angle potential E_{ANGLE} for atoms separated by two bonds is given by

$$E_{ANGLE} = k_\theta(\theta - \theta_{eq})^2 \tag{16}$$

where $k_\theta = 60$ kcal/mol rad^2 and $\theta_{eq} = 1.91$ rads (109.5°). The torsional or dihedral potential $E_{TORSION}$ for atoms separated by three bonds is given by

$$E_{TORSION} = \tfrac{1}{2}k_1(1-\cos(\varphi)) + \tfrac{1}{2}k_2(1-\cos(2\varphi)) + \tfrac{1}{2}k_3(1-\cos(3\varphi)) \tag{17}$$

where $k_1 = 1.62$ kcal/mol, $k_2 = -0.867$ kcal/mol, and $k_3 = 3.24$ kcal/mol. All interactions between atoms separated by three bonds are explicitly accounted for in the torsional potential. For atoms separated by more than three bonds and for atoms on different molecules, the non-bonded potential E_{BOND} is modeled by the Lennard–Jones relation:

$$E_{NONBOND} = 4\varepsilon[(\sigma/r)^{12} - (\sigma/r)^6] \tag{18}$$

where $\varepsilon = 0.112$ kcal/mol and $\sigma = 4.01$ Å, and with a 12 Å cut-off.

To model the secondary nucleation process specifically, we create two crystal surfaces on the x–y planes of the simulation cell. The crystal surface is modeled by an

exponential fit to the surface potential calibrated by Steele [39], using the Lennard–Jones parameters from the non-bonded interactions. The details of the surface potential are given in a previous paper [8]. The potential is periodic in the x-direction, with a wavelength of 4.33 Å, and in the y-direction with a wavelength of 2.5 Å. This creates a (110)-like surface that is corrugated in x and y. The y-direction corresponds to the c-axis of the crystal. The crystal exhibits hexagonal packing normal to the c-axis of the crystal. In Steele's formulation, the strength of the surface interaction is obtained by integrating over an infinitely thick crystal lattice, yielding an effective carbon–surface interaction that is stronger than the bare carbon–carbon interaction.

The simulations consist of 42 C50 chains, or 40 C100 in a box of fixed x- and y-dimensions. In the z-direction, the box dimension (the distance between the surfaces) is held at a constant stress of 1 atm, in order to accommodate the volume change associated with thermal contraction and crystallization. The initial box size for the C50 simulations is $25.9\times65.0\times39.3$ Å^3, and the initial configuration was generated at a reduced density of 0.3 g/cm^3 by growing each polymer chain with fixed bond lengths, fixed bond angles, and a torsional state of *trans*, *gauche plus* or *gauche minus*, selected according to probabilities generated from a Boltzmann weighting of the torsion angle potential at 400 K, discretized into the three rotational isomeric states. Overlap during chain construction was avoided by rejecting any steps that resulted in interatomic distances less than 5 Å during initialization; in the event that numerous unsuccessful attempts to grow a chain were encountered at the nth united atom, it was deleted and the process started again from the $n-1$'th atom, until all atoms were successfully placed. The simulation cell was then equilibrated to bulk density using molecular dynamics at 400 K and 1 atm for 1 ns. The C100 simulations started from a simulation cell that was $52.0\times80.0\times31.3$ Å^3, after being equilibrated for 1 ns at 500 K. After the equilibration phase, the systems were quenched below the melting point to begin the crystallization process. Identical C50 samples were quenched to 290, 300, 315, 330, 345 and 360 K. C100 samples were quenched to 350, 375 and 400 K.

For our previous study of C20 and for the simulation of C50 here, the y-dimension of the cell was readily chosen large enough to accommodate fully extended chains in the crystal phase, and fully extended chain crystallites were indeed observed to form, in accord with experimental observations. Full chain extension during crystallization has also been observed for C102 from solution at small undercoolings [40], but at the large undercoolings used here, the kinetics were expected to prevent the fully extended crystallization of C100 from occurring. Therefore, in the interest of shorter simulation time, the y-dimension of our C100 simulation is only 8 nm, sufficient to allow for the case of once-folded chains. However, our simulations were not run long enough to clearly resolve such integer-folded crystallites.

We integrate the equations of motion using the velocity–Verlet integration algorithm [41]. We use a 5 fs time step, which we have shown to be acceptable in our previous work. There is a 10% error in the magnitude of the bond and angle energies, which translates into a 10% increase in the relaxation times. The simulation is conducted at constant temperature, constant length in x- and y-dimensions, and constant stress of 1 atm in the z-dimension. Constant temperature and stress are maintained using velocity and position rescaling as described by Berendsen et al. [42]. The thermal inertial time constant τ_T and volume inertial time constant τ_P used were 3.3 ps and 5.0×10^3 ps, respectively. These inertial constants are relatively small, such that temperature and stress fluctuate little throughout the simulation. Crystallization kinetics are relatively insensitive to the values of these constants in this vicinity. Constant stress simulation is required to account for the volume change associated with crystallization. The thermostat ensures that the crystallization occurs under isothermal conditions. Justification for this type of thermostat can be demonstrated using a simple one-dimensional heat balance adapted from Eder et al. [43] in which all of the heat of crystallization is released to the melt. For values typical of C20 (melt thermal conductivity of 0.01522 W/m K, latent heat of crystallization of 16.9 kcal/mol, crystal density of 0.9361 g/cm^3 and crystal growth rate of 0.1 m/s), the temperature change over the length of a typical simulation cell does not exceed 10^{-3} K.

The standard measure of order used in polymer systems is the global bond orientation parameter at time t,

$$S(t) = \frac{3\langle[\nu_{\mathbf{i}}(t)\cdot\nu_{\mathbf{j}}(t)]^2\rangle}{2} - \frac{1}{2} \tag{19}$$

where $\boldsymbol{\nu}_{\mathbf{i}}(t)$ is the orientation vector of atom i at time t, defined by the chord from atom $i-1$ to atom $i+1$, and the average is taken over all pairs i and j. However, in order to calculate the spatial distribution of order within the simulation cell, a local orientation order must be defined, using convolutions of the local chain orientation vectors with spatial box functions.

The orientational order at a particular z-value and time is a function of the distribution of local order $\mathbf{f}_\nu(z,t)$ as described below,

$$\mathbf{f}_\nu(z,t) = \sum_{i=1}^{n} \nu_{\mathbf{i}}(t)\delta(z - z_i) \tag{20}$$

where z_i is the z-component of the position vector of atom i. For convolution, we use a box function $g(u_i)$

$$g(u_i) = \begin{cases} 0 & -\infty < u_i < -\dfrac{\mu}{2} \\ \dfrac{1}{\mu} & -\dfrac{\mu}{2} < u_i < \dfrac{\mu}{2} \\ 0 & \dfrac{\mu}{2} < u_i < \infty \end{cases} \tag{21}$$

where μ is the convolution width. The orientation order

density at z is computed by considering pairs of atoms within the range of the convolution width, $[z-\mu/2, z+\mu/2]$. This is done by convolving $\mathbf{f}_v(z,t)$ with $g(u_i)$ and $g(u_j)$, yielding

$$s(z,t) = \frac{3}{2}\left[\int_{-\mu/2}^{\mu/2}\int_{-\mu/2}^{\mu/2}\sum_{j=1}^{n}\sum_{i=1}^{n}(\nu_{\mathbf{i}}(t)\cdot\nu_{\mathbf{j}}(t))^2 \times\frac{1}{\mu^2}\delta(z-z_i-u_i)\delta(z-z_j-u_j)\mathrm{d}u_i\mathrm{d}u_j\right]-\frac{1}{2} \quad (22)$$

In order to obtain an average, analogous to the global orientational order parameter $S(t)$ in Eq. (19), we also need to know the density of pairs of beads at z at time t, given by $n(z,t)$, the convolution of an atomic distribution with $g(u_i)$ and $g(u_j)$:

$$n(z,t) = \int_{-\mu/2}^{\mu/2}\int_{-\mu/2}^{\mu/2}\sum_{j=1}^{n}\sum_{i=1}^{n}\frac{1}{\mu^2}\delta(z-z_i-u_i) \times\delta(z-z_j-u_j)\mathrm{d}u_i\mathrm{d}u_j \quad (23)$$

Now $S(z,t)$, the convolved orientational order parameter, is given by

$$S(z,t) = \frac{s(z,t)}{n(z,t)} \quad (24)$$

Choosing $\mu = L_z$, the simulation cell z-dimension, reduces Eq. (24) to the global bond order parameter $S(t)$, as defined in Eq. (19), while choosing a small value, such as $\mu = 0.5$ nm, as we have usually done, yields $S(z,t)$, the orientational order parameter at a particular location z at time t. An analogous convolution was performed in time over a 1 ns box function, using snapshots at 10 ps intervals, in order to filter fluctuations caused by individual bond and angle movements.

3. Results

3.1. Molecular dynamics simulations

Once the systems have been quenched below the melt temperature, the hallmarks of crystallization are almost immediately observable near the simulated surface, for both C50 and C100. Although these two systems manifest similarities, there are also some differences that can be immediately seen visually. Fig. 1(a) shows snapshots of the C50 system at times $t = 0$, 30, 60 and 90 ns after quenching to 330 K. Fig. 1(b) shows a similar set of snapshots for the C100 system at times $t = 0$, 20, 40 and 60 ns after quenching to 375 K. In both cases, the crystallization begins at the x–y walls of the simulation cell, where the simulated crystal surfaces (not shown) promote the addition of new crystal layers. As shown in Fig. 1(a), the typical C50 simulation first forms clearly defined, well-ordered layers of fully extended chains at the x–y boundaries of the cell, layering

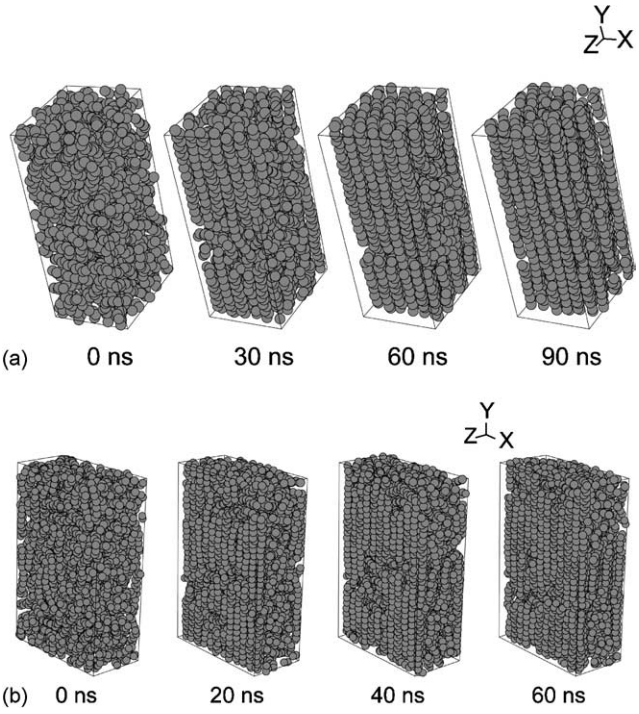

Fig. 1. Simulation cells for C50 and C100 systems, where simulated surfaces are located at the x–y walls; (a) chain configurations for the 42 C50 chain system quenched to 330 K at times $t = 0$, 30, 60, and 90 ns, (b) chain configurations for the 40 C100 chain system quenched to 375 K at times $t = 0$, 20, 40, and 60 ns.

which proceeds throughout the volume of the simulation cell. By 90 ns, the cell consists of 6 fully ordered crystalline layers. Fig. 1(b), however, reveals a somewhat different picture for crystallization of C100. The crystallization process still proceeds through a sequence of layer ordering stages starting at the x–y boundaries of the cell, but the progression is much slower. By 60 ns, the crystallization has not yet completely filled the simulation cell, and defects persist within all layers, including those nearest the Steele surface, until the end of the simulation. Rather than fully extended chains as seen in C20 and C50, or once-folded chains as seen experimentally near T_m in C100 at high undercoolings, only sections of chains are extended and packed.

The processes exemplified by Fig. 1 can be seen more clearly if viewed layer by layer. Fig. 2(a) shows the three layers closest to one surface of the cell, at various times for C50. With this view, we can see that two processes are occurring: ordering and extension of chains within a layer, and the propagation of that order from one layer to the next. For example, between 30 and 60 ns, the average length of chain residing entirely in layer 1, not counting short segments less than 10 beads long which appear to be melt-like loops, increases from approximately 20 to 50, through a process of drawing chains in from the melt. By 30 ns, one observes a band of partially extended, aligned, all-*trans* chain segments, approximately 20 CH2 segments

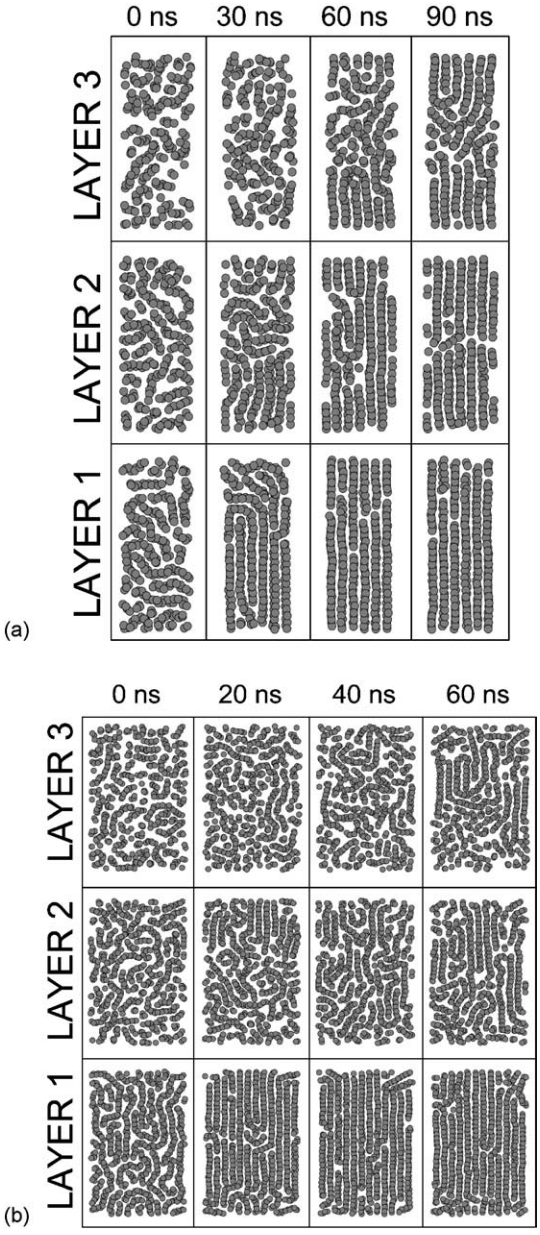

Fig. 2. (a) The three layers closest to $z=0$ plane for 42 C50 chains after quench to 330 K at $t=0$ ns. (b) The three layers closest to the $z=0$ plane for 40 C100 chains after quench to 375 K at $t=0$ ns.

long and 6 chains wide (the entire width of the cell in the x-dimension). In subsequent snapshots of the same layer, the chains become fully extended and the chain ends move into approximate registry through a process of chain sliding (longitudinal diffusion) within the layer. Simultaneously, in layer 2 at the next snapshot in time (60 ns), a similar band, 6 chains wide and 20 segments long overlays the ordered band in layer 1, and the process of perfection though chain sliding is repeated. A similar process appears to be occurring in layer 3 sometime between 60 and 90 ns. The ordering within a layer thus appears to be a stochastic process of drawing chains in from the melt, bringing them into crystallographic registry, and sliding them into different lattice positions to increase the stem length, over a period of 60 ns for each layer. *Gauche* states migrate away from the growing nucleus, until they either transform spontaneously into *trans* states or reach the chain end. Fig. 2(b) shows a similar sequence of events for C100. Although slower than in the C50 case and incomplete within the 60 ns of simulation, small regions of order approximately 20 CH2 segments long and 10 chains wide are nevertheless apparent in layer 1 in the 20 ns snapshot and proceed to lengthen within the layer in subsequent snapshots. In layer 2 at 60 ns, ordered regions approximately 20 CH2's long and 3 chains wide are only just apparent. Surface nuclei form on the regions of the previous layer that are crystalline.

We can estimate the distribution of partially extended chain segments, thereby identifying the distribution of the length of all-*trans* segments. We define a torsional state as a *trans* state if the torsional angle lies between $-\pi/3$ and $+\pi/3$, where the maximums in the *trans–gauche* barriers are. We use a convolution in time over a 1 ns box function to reduce fluctuations. Fig. 3(a) shows the distribution of sequences of consecutive *trans* torsions along a chain during the course of the simulation of C50 at 330 K. Initially, the *trans* torsional states are distributed in segments of length ten CH2's or shorter. With time, this distribution shifts towards a population around 22 CH2's long, through accretion of approximately 3 beads every 4 ns. This process of addition of beads appears to be stochastic over a period of 60 ns, by which time long-lived populations of all-trans segments $\sim$22 and 50 CH2's long are established. Remarkably, at later times the shift in the distribution to fully extended chains 50 CH2's long occurs in a single, large step, with very few all-*trans* segments of intermediate length. This indicates that the jump from chain segments of 20 to 50 is activated, so that there is not a gradual shift in the entire population of the stems as might be expected for a diffusion-like process, but rather individual stems or groups of stems grow in size fast enough that we do not observe significant numbers of intermediate length stems over any appreciable time.

In contrast to the C50 case shown in Fig. 3(a), the picture suggested by Fig. 3(b) for the crystallization in C100 at 375 K is slightly different. Here too there appears to be a stochastic process of accretion of all-*trans* segments over a 60 ns period. There remain a large number of short stems throughout the course of the simulation, and the population of longer stems is slow to develop; there is only a small population of chains that have extended the full y-dimension of the simulation cell, around 60 beads long. By the end of the simulation, however, a peak for stems of length 20 does appear to be developing, but the simulation is not long enough to observe the increase in this population or any subsequent activated jumps to longer all-*trans* segments.

In order to quantify this series of events, we evaluate the order parameter $S(z,t)$ for each layer. This is accomplished by evaluating Eq. (20) at $z=0.45$, 0.85 and 1.25 nm from the x–y boundary for layers 1, 2 and 3, respectively,

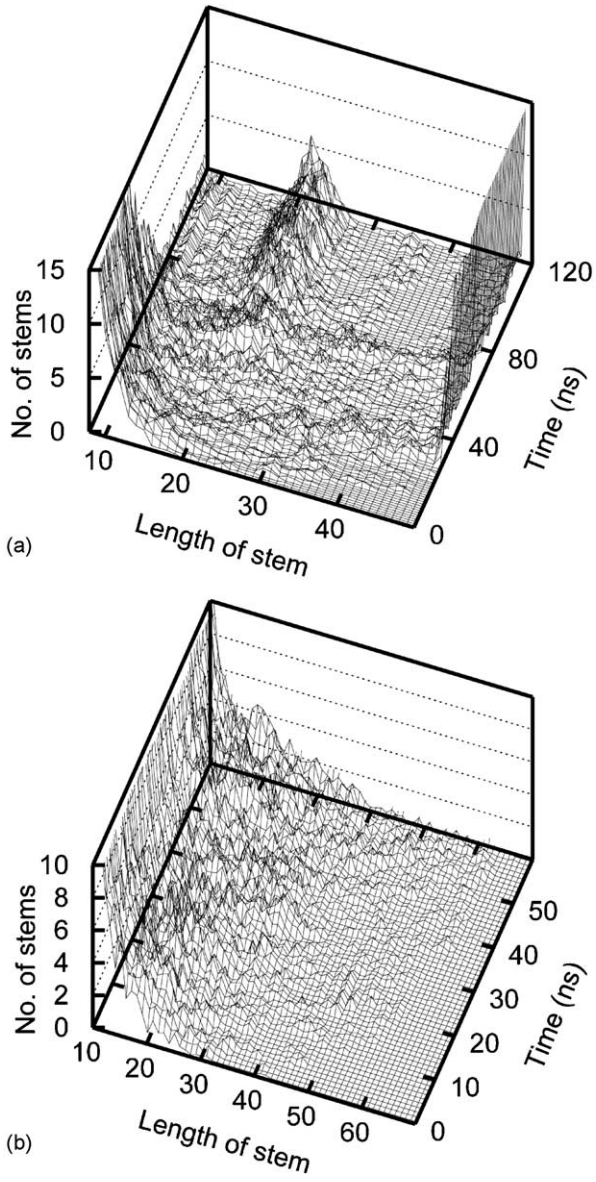

Fig. 3. Distribution of all-*trans* stem segments over time for (a) 42 C50 chains quenched to 330 K at $t=0$ ns; (b) 40 C100 chains quenched to 375 K at $t=0$ ns.

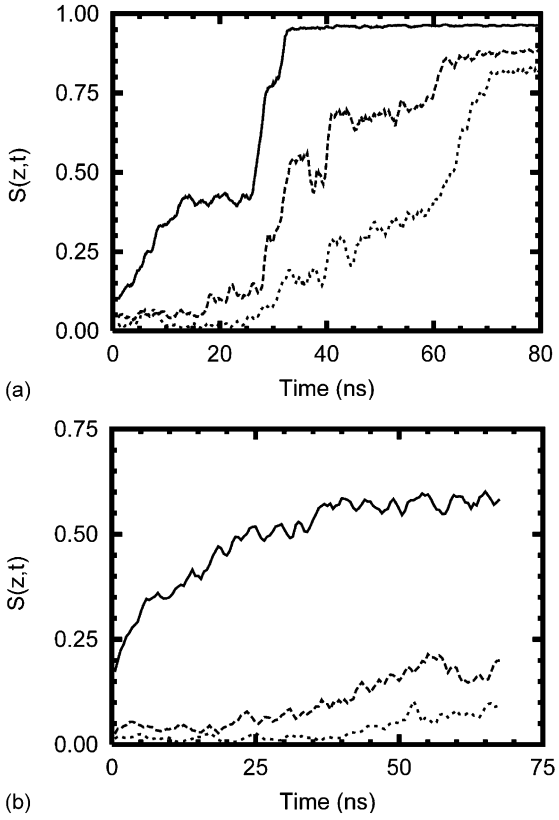

Fig. 4. Local order parameter $S(z,t)$ as a function of time, over the convolution width of 0.40 nm, at the locations of the three layers closest to the simulated surface: $z=0.45$ nm (layer 1, solid line); $z=0.85$ nm (layer 2, dashed line); $z=1.25$ nm (layer 3, dotted line); for (a) 42 C50 chains quenched to 330 K at $t=0$ ns; (b) 40 C100 chains quenched to 375 K at $t=0$ ns.

with a convolution width μ of 0.4 nm. Fig. 4(a) shows the results of this analysis over time for the first 3 layers for the C50 case. Full ordering of the first layer is accomplished in two stages, the first occurring between 0 and 15 ns, and the second between 25 and 35 ns. Ordering in the second layer begins concurrent with the second stage of layer 1. The large increase in $S(z,t)$, as it approaches its equilibrium crystalline value for a given layer, is in part due to the increased mobility of the chain ends, which are the last segments to be drawn into the layer, and in part because as $S(z,t)$ approaches one, the layer is almost filled, and the periodic boundaries enhance the stability of the ordered layer. Because of the small system size, fluctuations in $S(z,t)$ reflect the conformational changes in individual stems; in a larger simulation, we would expect these fluctuations to be damped, as is the case in the larger C100 simulations, shown in Fig. 4(b). One might expect the existence of a critical nucleus size for secondary nucleation to be reflected in a critical value for $S(z,t)$, but this is not obvious from Fig. 4. Such a critical value, if it existed, would be different for the C50 and C100 simulations in any case, since the x–y dimension differs for these two simulations ($S(z,t)$ is normalized by the total number of beads in a layer, Eq. (24)). For the C100 case, we never observe a fully oriented layer due to the fact that the y-dimension is only 8 nm, sufficient only to accommodate stems up to length 60 CH2's without a defect. Thus, the dynamics of stem growth only up to 1/2 the fully extended chain length can be studied in this case. For this reason, the C100 simulation only obtains a value for $S(z,t)$ of around 0.55, indicating that part of the layer does not crystallize. The behavior in this region is analogous to the impingement of two surface nuclei, which has been observed by Yamamoto [7].

The two different processes seen in Fig. 2, ordering within a layer, and propagation of that order to the next layer, can be quantified clearly in a three dimensional plot of the order parameter $S(z,t)$ versus distance and time. Fig. 5(a)

shows the profile of the orientation parameter $S(z,t)$, using a convolution width of 0.5 nm. It reveals the growth front for the C50 system after quench to 330 K, and its movement with time. Initially, the simulation cell begins from an amorphous state, and $S(z,t)$ is approximately zero throughout the cell. As the simulation progresses, order develops first near the z-boundaries, as evidenced by the rise in $S(z,t)$ near $z=0$ and 3.35 nm, and then propagates towards the centerline of the cell. The growth front can be identified as the z-region through which $S(z,t)$ makes the transition from amorphous to crystal. Fig. 5(b) shows the orientation profile $S(z,t)$ as a function of time for the C100 system after quenching to 375 K. The movement of the orientation front is slow but steady. The asymptotic limit of $S(z)$ is near 0.90, as the layers always contain some amount of disorder as the stems impinge on themselves in the y-direction.

This order profile can be fit by a hyperbolic tangent function, as described previously [8]. Since, there are two surfaces in the simulation cell, there are two growth fronts moving towards each other. The entire z-profile, including both growth fronts, can be modeled with two hyperbolic tangents, as follows,

$$S(z) = \tfrac{1}{2}\left[H_1 + H_2 - (H_1 - h)\tanh(\lambda_1(x-\xi_1)) + (H_2 - h)\tanh(\lambda_2(x-\xi_2))\right] \quad (25)$$

where H_i is the asymptotic value of the order parameter for the crystal growing at surface i, h is the asymptotic value of the order parameter for the amorphous region between the crystals, $1/\lambda_i$ is the interfacial width of phase boundary i, and ξ_i is the inflection point of phase boundary i. Fitting is done using a Levenberg–Marquardt non-linear least squares algorithm. The movement of the inflection point ξ_i is approximately linear in time, in accord with experiments on spherulites. The growth rate is given by the average value of $d\xi_i/dt$.

Approximately 75% of the change in the order parameter between crystal and melt occurs in the z-region $[\xi-(1/\lambda), \xi+(1/\lambda)]$. The width of the interface should be that of a single layer if growth resembles regime I or II in Hoffman's analysis. Regime III growth occurs over many layers, and should be reflected in a larger interfacial width. If a crystal grows a single layer at a time, then the interfacial width remains small. However, if there are multiple layers of surface nuclei with terraces and holes to be filled, it will take a larger value. Fig. 6 shows the time-averaged value of interfacial width $1/\lambda$ versus temperature for both C50 and C100. Both sets of data follow the same trend, decreasing in interfacial width with increasing temperature. In addition, it is worth noting that the standard deviation from the average value, which is a measure of the variability of the surface roughness, shown by the error bars, is much less for C100 than for C50.

Using this analysis we can also measure the growth rates for our simulations. We discard growth rates obtained at very short times, where the static nature of the Steele potential artificially accelerates the growth rate, and at very

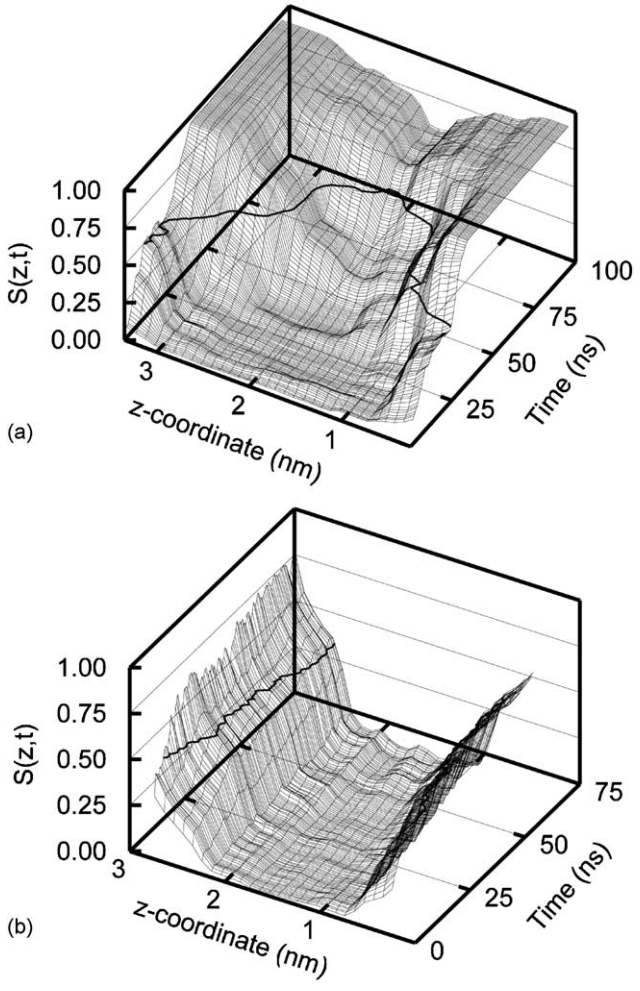

Fig. 5. Progression of the orientational order $S(z,t)$ growth front for (a) 42 C50 chains quenched to 330 K at $t=0$ ns, and (b) 40 C100 chains quenched to 375 K at $t=0$ ns. The z-coordinate is the direction normal to the surface. The convolution width is 0.5 nm. In each case, the contour at which the order parameter is halfway between the crystal and melt values is highlighted.

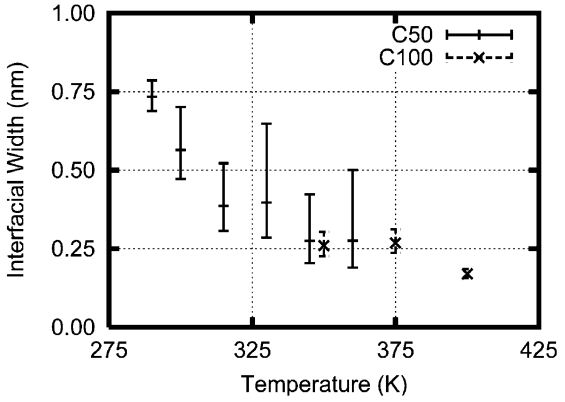

Fig. 6. The average interfacial width of the growth front, as given by $1/\lambda_i$ in Eq. (25), as a function of temperature for the 42 C50 chain systems (+) and the 40 C100 systems (×); error bars show standard deviations.

long times, where impingement of the surfaces occurs; the data presented are only in the range where the inflection point ξ_i in Eq. (25) is farther than the Lennard–Jones cut-off length from either of these singularities. The movement of the inflection points of the two growth fronts yields two measures for the linear growth rate normal to the surfaces, each one based on a linear fit to the front location versus time. For C50, identical samples quenched to 285, 290, 300, 315, 330, 345 and 360 K provided data for the growth rate as a function of temperature shown in Fig. 7, which reveals a maximum in the growth rate near 347 K for C50. When we apply the same analysis to the C100 systems, we obtain the growth rates shown in Fig. 7 at each of the three temperatures we simulated, with a maximum growth rate occurring near 395 K. Previously obtained data for C20 [8] is also plotted in Fig. 7 for comparison.

3.2. Crystallization rate model

In order to parameterize the crystallization rate model presented above, a total of seven unknown parameters need to be determined. There are three parameters in Eq. (11), related to the rate processes, G_0, C, and n. The parameter m is assigned the value of 2 or 3 depending on whether Rouse dynamics or reptation dynamics are assumed. There are also four parameters in Eqs. (12) and (13) that capture the molecular weight dependence of the phase transition temperatures: T_g^∞, C_g, T_m^∞ and C_m. In addition, we take C20 as the reference, which gives G_0 the interpretation of the value for the diffusion-limited rate pre-factor for C20 at its T_g, which is expected to be a small value. We performed the seven parameter fit to Eq. (11) with Eqs. (12) and (13) for T_m and T_g, respectively, using a Levenberg–Marquardt non-linear least squares algorithm, with the standard error propagation based on the uncertainty in the simulated growth rates. The resulting parameters and their standard deviations are given in Table 1 for both the Rouse and the reptation assumptions, and the best fit curves are plotted in Fig. 7. Because G_0 can change orders of magnitude during the fitting process, it is fitted as an exponential, and the standard deviation presented is the standard deviation of the exponent. Data near the maximum crystallization rate is better described by the curve, partly due to the lower statistical error associated with the determination of these values by molecular dynamics. Relative to the model with Rouse dynamics, the model with reptation dynamics compensates for the exponential factor $m=3$ by increased values of C and n, and a widening of the envelope in which crystallization takes place, which evidenced by the T_g and T_m values in Table 2 for each model.

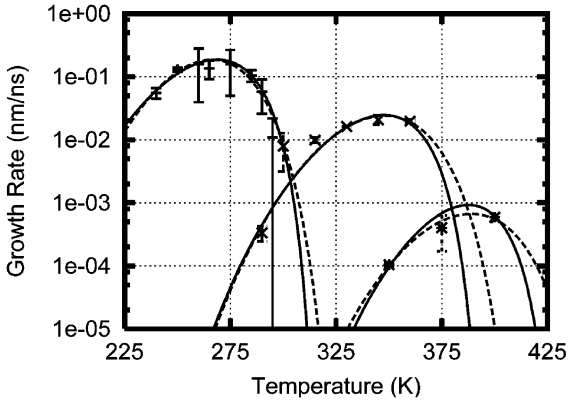

Fig. 7. Temperature dependence of growth rates, based on orientational order, calculated from the movement of ξ_i in Eq. (25). Average growth rates are shown for the 102 C20 chain systems (+), the 42 C50 chain systems (×), and the 40 C100 chain systems (*); individual growth rates obtained for each surface are indicated by error bars. Lines show the fit of the model equation, Eq. (11), to the growth rate data for each molecular weight, assuming Rouse dynamics (solid lines) and reptation dynamics (dashed lines).

Table 1
Calculated parameters, and their standard deviations, for the model given by Eqs. (11)–(13), assuming Rouse dynamics or reptation dynamics, for the fits in Fig. 7

Parameter	Rouse dynamics		Reptation dynamics	
	Value	SD	Value	SD
$\ln(G_0$ [m/s])	−37.9	16.1	−41.3	15.5
C [K]	439	197	855	217
n	1.49	0.44	1.79	0.43
T_m^∞ [K]	500	11	535	8
T_g^∞ [K]	346	36	302	43
C_m [CH2·K]	4.78×10^3	398	5.46×10^3	468
C_g [CH2·K]	1.24×10^4	1224	8.70×10^3	1840

Error analysis was conducted on the fits for the Rouse and reptation models to determine if the difference in the fits is statistically significant. The individual residual errors of the fit were normalized by the measurement error at each data point. Then a paired Student's t-test was conducted on the sample of 17 normalized errors using each model. The resulting probability of the null hypothesis is 0.108, indicating that the difference between the two models is not statistically significant.

4. Discussion

Before discussion of these results, it should be reiterated that the late stage of crystallization and completion of ordering in each layer may be affected by the finite size of

Table 2
Values of the glass transition and melting temperatures, given by Eqs. (12) and (13), for the model fits shown in Fig. 7, for both the Rouse dynamics assumption and the reptation dynamics assumption

Length	Rouse		Reptation	
	T_g (K)	T_m (K)	T_g (K)	T_m (K)
20	124	338	124	354
50	201	420	192	444
100	254	457	235	485

the simulation cells, so the structure and dynamics of layer completion are not analyzed in detail here. However, finite size effects are expected to exert less influence on the early stages of crystallization and initial ordering in each layer. As mentioned in Section 3, the surface nucleus is small and should not be affected by the periodic boundaries. In addition, the development of the secondary nucleation event in the subsequent layer occurs prior to completion of ordering in the underlying layer, and thus should also not be affected by finite size effects. Based on this observation, we conclude that the simulated growth rates are only weakly sensitive to finite size effects in these simulations.

The two models based on Rouse dynamics and reptation dynamics were statistically equivalent fits to the data. However, we can make some logical conclusions based on the values of the fitting parameters for the two models. Particularly noteworthy is the value of C in the reptation case, which is much larger than what is typically observed in nucleation-limited experiments. In addition, the predictions for the melt temperatures in the Rouse-based model, given in Table 2 are closer to the experimentally observed values than in the reptation-based model. In earlier work [8], we obtained a melting temperature of 345 K for C20 by direct simulation, 35 K higher than the experimental value of 310 K. Glass transition temperatures are more difficult to obtain, but recent simulation results with a similar potential suggest a T_g of 280 ± 32 K for a C768 chain [44]. Thus, direct simulation overestimates these quantities by about 30 K, which can be attributed to limitations of the force field and the simulation methods. Parameter-fitting of the crystallization rates using the Rouse-based mode, on the other hand, over-predicts the melting temperatures of C20, C50 and C100 by 30–70 K, relative to the experimental values (310, 365 and 388 K, respectively). Extrapolation of the parameter fit for Eq. (12) to C768 yields a T_g of 330, 50 K higher than the simulated value. The larger errors in T_g and T_m arising from parameter fitting can, therefore, be attributed to approximations of the analytical model rather than to errors in the simulations (or simulated growth rates) themselves. Interestingly, the temperatures at which the crystal growth rate is maximal according to the simulation accords well with the '2/3' rule of thumb when considered in relation the glass transition and melting temperatures listed in Table 2.

The interfacial width appears to be mainly a function of temperature, rather than supercooling, with interfacial width decreasing as temperature increases. The width of the interface does not appear to depend explicitly on molecular weight. However, because higher molecular weight polymers have higher melting temperatures and glass transition temperatures, the envelope in which they crystallize is shifted to higher temperatures. Therefore, our MD results suggest that higher molecular weight polymers would tend to have sharper interfaces. The decrease of the interfacial width with temperature reveals the gradual departure from 'rough' or 'normal' growth, where there are multiple layers of nucleation, to 'layer' growth, where a single nucleation site occurs in a layer, and growth occurs mainly through addition on the terraces of that site. As temperature increases, the interfacial width seems to level off around 0.25 nm, i.e. 75% of the change in the order parameter occurs in a single layer. In the high temperature cases, it seems that the process of removal of chains that have locked into registry is energetically more likely, which leads to a more ordered growth front. This is similar to a transition from Hoffman's rough regime III growth, to the more ordered regime II. Comparing the results for C50 and C100 in Fig. 6, the longer chains crystallize fastest in the temperature range where interfacial width is approximately constant.

Some of the observations made regarding the mechanisms of ordering and propagation have implications for secondary nucleation theory for alkanes and polymers. Lauritzen and Hoffman assumed that the critical rate-limiting step was a stem segment extending to a length matching the underlying lamellar thickness or, in later work, an adsorbed but unattached segment. In turn, they parameterized the thermodynamics of this in terms of the surface energy of the lateral surfaces and fold surfaces associated with these steps. Estimates for the fold energy of a polymer lamella are often made by applying this assumption to measurements of spherulitic growth rates. We have not seen any evidence of this full-length extended stem nucleation; we observe the initial formation of surface nuclei of stems of length 20. Similarly, Mandelkern's assumption of a monomolecular surface nucleus is also not supported by these simulations; instead, we observe a surface nucleus that involves several segments of different chains locking into surface registry. This different picture of growth has implications for the determination of surface energies from the thermodynamic constant C.

We observe multiple chains adsorbing and desorbing on the crystal surface. When a group of chains adsorb onto the surface stochastically in the same area, a critical nucleus may be formed. Although the nature of this surface nucleus is difficult to characterize precisely, there are some comments we can make based on general observation. This surface nucleus does not involve chains extended to the length of the underlying surface. It typically consists of a group of chains that are 20–24 beads long and 4–5 chains across at $T = 330$ K (C50) or $T = 375$ K (C100), corresponding to the low temperature side of the growth rate curve. This is in close agreement with predictions by Wagner and Phillips [45] who estimated that the critical nucleus size for polyethylene is 3–4 stems at $T = 392$ K, based on rate measurements for polyethylene and ethylene–octene copolymers. The stability of this critical nucleus depends on the extra surface the nucleus has created, as Hoffman and Mandelkern postulated from classical nucleation theory, but it also depends on the number of defects within the nucleus, and the topology of the melt to which the monomer beads in the surface nucleus are connected. It is difficult to conclude

whether the nucleation occurring on the surface is that of a mesomorphic or metastable phase, as Strobl and Keller have suggested, or whether the nucleus is temperature-dependent; qualitatively, we did not observe significant differences in the surface nucleus at the different crystallization temperatures. Nevertheless, it appears essential that the initial nucleus is shorter than the fully extended stem length in the final crystal and that it involves multiple chains. The united atom force field used here crystallizes in a hexagonal form, which exhibits the same symmetry as the proposed mobile rotator phase in polyethylene. Binsbergen's assertion that polymer crystal growth is stochastic, involving several addition and removal steps, may be applicable not only to the addition and removal that creates a critical nucleus, but also to the sliding movement of the chains that allows thickening after the critical nucleus is formed. Growth of a nucleus consisting of a group of chain segments involves reorganization of the initial nucleus.

The energy of the fold surface of the lamella is often assumed to be the energy of the 'fold' surface of the surface nucleus, based on the fact that this is the surface through which chain connectivity is maintained. However, this surface of the surface nucleus does not compare well with the lamellar fold surface. As surface nucleation occurs, there do not appear to be any recognizable 'folds'. The energy of that surface can be better characterized as the energy associated with changing the torsional conformation of the chain from the crystalline all-trans state, to the Boltzmann-weighted torsional states of the melt. It seems that it is not until later that the final thickness of the crystal layer fully develops. Thus, the surface nucleus we observe is instrumental in determining the crystal growth rate, but it may not determine the final lamellar thickness in polymer crystals. In our C50 simulations the chains eventually extend fully, while in the C100 simulations, they are limited by impingement of the chains on their periodic image.

The model seems to capture the behavior of crystallization rates well. It is less useful as means for determining transition temperatures. Melting points can be calculated from Monte Carlo simulations; both melting points [3] and glass transition points [44] have been estimated using molecular dynamics simulations. However, a larger number of simulations would be required to capture the molecular weight dependence effectively.

In addition to the crystallization model presented here, we have also tested some of the models available in the literature against our simulation data. We have fit the equations of van Krevelen, Strobl, and Umemoto to our C20, C50, and C100 data independently, and found that they too capture the temperature dependence adequately. We have checked these models for their molecular weight dependence as well. Umemoto's equations require an empirical relationship for the maximum growth rate as a function of molecular weight. Umemoto suggested a power law dependence for this relationship [29], but based on our simulation data, a power law relation does not capture the

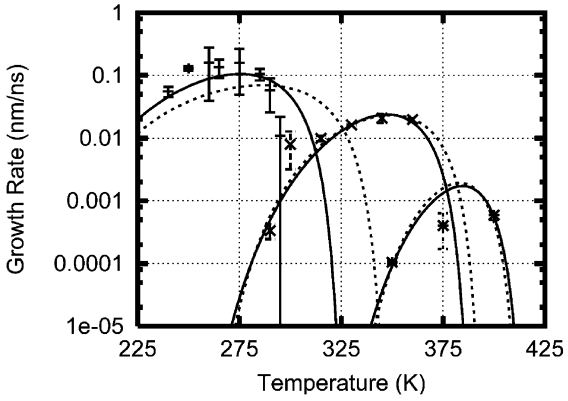

Fig. 8. Best fit equations for other growth rate models as a function of temperature and molecular weight (lines), for the growth rate data shown: the 102 C20 chain systems (+), the 42 C50 chain systems (×), and the 40 C100 chain systems (*). Molecular weight dependence is incorporated through the transition points using Eqs. (12) and (13), as in our model: van Krevelen's model (solid lines); Strobl's model (dashed lines).

molecular weight dependence of the maximum growth rate in this range. Fig. 8 show a comparison of all our simulation data at all three molecular weights to the best fit models of van Krevelen [16] and Strobl [24]. Neither model includes any explicit molecular weight dependence, but there is an implicit dependence on molecular weight via the glass transition temperature and the melting temperature. While data at each molecular weight can be fit independently, Fig. 8 shows that the neither of these models can fit the entire range of data; there needs to be an additional contribution due to molecular weight. The Rouse-based alkane model, however, predicts reasonable trends in the crystal growth rate as a function of molecular weight and temperature; this is shown in Fig. 9.

Validation of these results from experimental observation is difficult, since our timescale of observation is much shorter than that of experimental methods. However, experimental and computational methods are beginning to converge towards the same timescale. Recent works on high speed crystallization have been able to measure crystallization rates for polyethylene over a wide range of

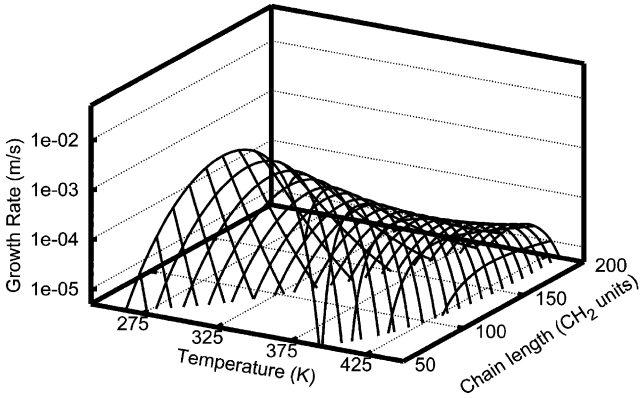

Fig. 9. The effect of molecular weight and temperature on growth rates, predicted by our model equation Eq. (11), for Rouse dynamics.

temperatures from the melting temperature to near the temperature where the maximum rate occurs [45,46]. It is worth noting that our predicted maximum crystallization rate for C100 is on the order of 10^{-3} m/s, while experiments indicate a maximum crystallization rate for polyethylene on the order of 10^{-4} m/s. This is in the range of our model extrapolations for the 150–200 chain length, as seen in Fig. 9. Beyond the entanglement length (approximately 150–200 beads), we do not expect that Rouse dynamics should be applicable; rather, reptation dynamics should come into play. However, the relatively weak molecular weight dependence of the maximum growth rate beyond the onset of entanglements and agreement between the predictions of our model for chains in the entangled regime and the experimental data for polyethylene suggest that the conformational relaxation of the length of the entangled segment may be the relevant kinetic barrier for high molecular weight polymers at large undercoolings.

5. Conclusions

In summary, we have constructed a crystallization model that can be quantified entirely in terms of universal properties of polymer chains and chemically specific quantities that can be estimated polymer by polymer by molecular simulation. Furthermore, we have for the first time parameterized a crystallization model using molecular dynamics simulations. The model predicts crystal growth rates as a function of temperature and molecular weight up to the entanglement molecular weight. We have studied polymer crystal growth for C50 and C100 with non-equilibrium molecular dynamics. Using techniques we have developed to measure growth rates based on orientational order, we have been able to quantify growth rates and make qualitative comments about the likelihood of secondary nucleation mechanisms. Error analysis reveals that there is no statistically significant difference between the Rouse-based model and a reptation-based model, but the thermodynamic parameters for the Rouse-based model are closer to those measured empirically.

Acknowledgements

This work was supported by the Center for Advanced Engineering Fibers and Films (CAEFF) of the Engineering Research Centers Program of the National Science Foundation, under NSF Award Number EEC-9731680.

References

[1] Koyama A, Yamamoto T, Fukao K, Miyamoto Y. Phys Rev E 2002; 65(5) [Art. No. 050801].
[2] Lavine MS, Waheed N, Rutledge GC. Polymer 2003;44(5):1771–9.
[3] Meyer H, Muller-Plathe F. Macromolecules 2002;35(4):1241–52.
[4] Fujiwara S, Sato T. J Chem Phys 1999;110(19):9757–64.
[5] Hu WB, Frenkel D, Mathot VBF. Macromolecules 2003;36(3): 549–52.
[6] Shimizu T, Yamamoto T. J Chem Phys 2000;113(8):3351–9.
[7] Yamamoto T. Polymer 2004;45(4):1357–64.
[8] Waheed N, Lavine MS, Rutledge GC. J Chem Phys 2002;116(5): 2301–9.
[9] Hoffman JD, Weeks JJ. J Chem Phys 1962;37(8):1723–41.
[10] Mandelkern L. Crystallization of polymers. New York: McGraw-Hill; 1964.
[11] Nozaki K, Hikosaka M. In: Garti N, Sato K, editors. Crystallization processes in fats and lipid systems. New York: Marcel Dekker; 2001. p. 151–76.
[12] Mandelkern L. Proceedings of the international conference on crystal growth. New York: Wiley; 1958. p. 467–95.
[13] Ziabicki A. Fundamentals of fibre formation. London: Wiley; 1976.
[14] Gandica A, Magill JH. Polymer 1972;13:595–6.
[15] Umemoto S, Okui N. Polymer 2002;43(4):1423–7.
[16] van Krevelen DW. Chimia 1978;32(8):279–94.
[17] Hoffman JD, Miller RL. Polymer 1997;38(13):3151–212.
[18] Lauritzen JI, Hoffman JD. J Appl Phys 1973;44(10):4340–52.
[19] Armistead JP, Hoffman JD. Macromolecules 2002;35(10):3895–913.
[20] Binsbergen FL. Kolloid Zeitscrift 1970;237:389–95.
[21] Point JJ. Macromolecules 1979;12(4):770–5.
[22] Sadler DM, Gilmer GH. Phys Rev Lett 1986;56(25):2708–11.
[23] Keller A, Hikosaka M, Rastogi S, Toda A, Barham PJ, Goldbeck-Wood G. J Mater Sci 1994;29(10):2579–604.
[24] Strobl G. Eur Phys J E 2000;3(2):165–83.
[25] Turnbull D, Fisher JC. J Chem Phys 1949;17(1):71–3.
[26] Gibbs JW. The collected works of J. Willard Gibbs. vol. 1. New Haven, CT, USA: Yale Univ. Press; 1948.
[27] Mandelkern L, Jain NL, Kim H. J Polym Sci A2 1968;6:165–80.
[28] Van Antwerpen F, van Krevelen DW. J Polym Sci Part B: Polym Phys 1972;10(12):2423–35.
[29] Umemoto S, Kobayashi N, Okui N. J Macromol Sci Phys 2002; B41(4–6):923–38.
[30] Hoffman JD, Frolen LJ, Ross GS, Lauritzen JI. J Res Natl Bur Stand A Phys Chem 1975;79(6):671–99.
[31] DeGennes PG. Macromolecules 1981;14(6):1637–44.
[32] Semenov AN, Joanny JF. J Phys II 1995;5(6):859–76.
[33] Sukhishvili SA, Chen Y, Muller JD, Gratton E, Schweizer KS, Granick S. Nature 2000;406(6792):146.
[34] Ferry JD. Viscoelastic properties of polymers. New York: Wiley; 1970.
[35] Williams ML, Landel RF, Ferry JD. J Am Chem Soc 1955;77:3701–7.
[36] Fox TG, Loshaek S. J Polym Sci 1955;15:371–84.
[37] Small DM. The physical chemistry of lipids: from alkanes to phospholipids. New York: Plenum Press; 1986. p. 183–232.
[38] Paul W, Yoon DY, Smith GD. J Chem Phys 1995;103(4):1702–9.
[39] Steele WM. Surf Sci 1973;36:317–52.
[40] Ungar G, Stejny J, Keller A, Bidd I, Whiting MC. Science 1985; 229(4711):386–9.
[41] Swope WC, Andersen HC, Berens PH, Wilson KR. J Chem Phys 1982;76(637):648.
[42] Berendsen HJC, Postma JPM, Van Gunsteren WF, Dinola A, Haak JR. J Chem Phys 1984;81(8):3684–90.
[43] Eder G, Janeschitz-Kriegl H, Liedauer S. Prog Polym Sci 1990;15(4): 629–714.
[44] Capaldi FM, Boyce MC, Rutledge GC. Polymer 2004;45(4):1391–9.
[45] Wagner J, Phillips PJ. Polymer 2001;42(21):8999–9013.
[46] Ratajski E, Janeschitz-Kriegl H. Colloid Polym Sci 1996;274(10): 938–51.